In situ construction of an ultra-robust and lithiophilic Li-enriched Li-N nanoshield for high-performance Ge-based anode materials

Bing-Qing Xiong[1,†], Xinwei Zhou[3,4,†], Gui-Liang Xu[2,*], Xiang Liu[2], Youcheng Hu[1], Yuzi Liu[3], Likun Zhu[3], Chen-Guang Shi[5], Yu-Hao Hong[5], Si-Cheng Wan[1], Cheng-Jun Sun[6], Shengli Chen[1], Ling Huang[5], Shi-Gang Sun[5], Khalil Amine[2,7,8,*] & Fu-Sheng Ke[1,*]

[1]Sauvage Center for Molecular Sciences, College of Chemistry and Molecular Sciences, Wuhan University, Wuhan 430072, China

[2]Chemical Sciences and Engineering Division, Argonne National Laboratory, Lemont, IL 60439, USA

[3]Center for Nanoscale Materials, Argonne National Laboratory, Lemont, IL 60439, USA

[4]Department of Mechanical and Energy Engineering, Indiana University-Purdue University Indianapolis, Indianapolis, IN 46202, USA

[5]State Key Laboratory of Physical Chemistry of Solid Surfaces, Department of Chemistry, College of Chemistry and Chemical Engineering, Xiamen University, Xiamen 361005, China

[6]X-ray sciences division, Argonne National Laboratory, Lemont, IL 60439, USA

[7]Materials Science and Engineering, Stanford University, Stanford, CA 94305, USA

[8] IRMC, Imam AbduIrahman Bin Faisal University (IAU), Dammam, 34212, Saudi Arabia

Corresponding Author

*xug@anl.gov (G. -L. Xu), *amine@anl.gov (K. Amine), and *kefs@whu.edu.cn (F. -S. Ke)

This is the author's manuscript of the article published in final edited form as:

Xiong, B.-Q., Zhou, X., Xu, G.-L., Liu, X., Hu, Y., Liu, Y., Zhu, L., Shi, C.-G., Hong, Y.-H., Wan, S.-C., Sun, C.-J., Chen, S., Huang, L., Sun, S.-G., Amine, K., & Ke, F.-S. (2020). In Situ Construction of an Ultrarobust and Lithiophilic Li-Enriched Li–N Nanoshield for High-Performance Ge-Based Anode Materials. ACS Energy Letters, 5(11), 3490–3497. https://doi.org/10.1021/acsenergylett.0c02121

ABSTRACT: Alloy-based materials are promising anodes for rechargeable batteries thanks to their higher theoretical capacities than graphite. Unfortunately, the huge volume changes during cycling cause serious structural degradation and undesired parasitic reactions with electrolytes, resulting in fragile solid-electrolyte interphase formation and serious capacity decay. This work proposes to mitigate the volume changes and suppress the interfacial reactivity of Ge anodes without sacrificing the interfacial Li^+ transport, through in situ construction of an ultra-robust and lithiophilic Li-enriched Li-N nanoshield, which demonstrated improved chemical, electrochemical, mechanical, and environmental stability. Therefore, it can serve as a versatile interlayer to facilitate Li^+ transport and effectively block the attack of electrolyte solvents, thus boosting the long-term cycle stability and fast charging capability of Ge anodes. This work offers an alternative methodology to tune the interfaces of other electrode materials as well by screening for more N-containing compounds that can react with Li^+ during battery operation.

TOC GRAPHICS

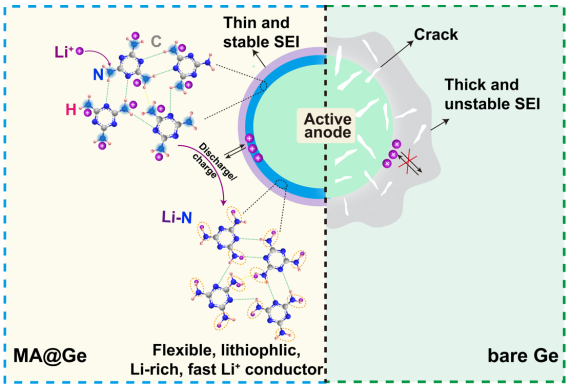

Alloy-based materials MM' (M=Li; M'=P, Ge, Sb, Sn, Si, etc.) are regarded as appealing

anodes for high-energy lithium-ion batteries thanks to their higher theoretical capacities than graphite anodes.[1,2] However, the alloying/de-alloying processes of these anodes are accompanied by large volume changes (up to 400%), which not only cause the pulverization and insulation of active materials during cycling, but also cause undesired electrolyte decomposition on the newly exposed particle surfaces. Both processes result in the generation of thick solid-electrolyte interphase (SEI) and depletion of electrolytes, eventually causing fast capacity degradation.[3,4] To overcome these problems, most efforts have been focusing on utilization of nanometer-sized materials with various morphologies.[5,6] However, their commercial application has long been hindered by their low tap density and low initial Coulombic efficiency associated with nanomaterials. An alternative strategy is interface engineering, which can tune the compositional and mechanical character of the SEI. The SEI plays vital roles in many electrochemical systems, such as alloy and metal anodes. It is generally made up of multicomponent organic (e.g., $ROCO_2Li$, $(CH_2OCO_2Li)_2$, and polycarbonates) and inorganic (LiF, Li_2CO_3, Li_2O, and LiOH) phases. An ideal SEI with good chemical and mechanical stability, high ionic but low electronic conductivity is necessary to enable the durable operation of battery materials especially for alloy-based anode materials.[7,8]

Significant progress has been made in constructing robust SEI via functional additives,[9] salt-concentrated electrolytes,[10] Li salt and solvent optimizations.[11] Most of them could result in the formation of a LiF-enriched SEI, which has recently gained popularity especially for Li metal batteries. This is because LiF exhibits robust chemical stability against Li metal/liquid electrolytes and good electrochemical stability. For example, salt-concentrated electrolyte is a promising strategy to obtain a LiF-enriched SEI owing to the significantly reduced free solvent molecules activities.[11-13] On the other hand, our group has recently found that tuning surface structures of Ge and Si by selective catalytic decomposition of electrolyte additives is another promising way to form the LiF-enriched SEI for alloy-based anodes and maximize their cycle life.[14] However, the ionic conductivity of LiF itself is very low ($<10^{-9}$ S cm^{-1}) and becomes

even worse when the formed LiF has a homogeneous and dense structure,[7,15,16] which would dramatically jeopardize the fast charging capability of the batteries.[17] Moreover, He et al. have recently reported that the mechanical strength of a LiF-enriched SEI is not robust enough to prevent the breakdown process during cycling, especial for alloy-based anodes with large volume changes.[18] Therefore, there is an urgent need to explore a novel interface that can mitigate the aforementioned issues.

In addition to the fluorinated SEI, the Li_3N-dominated interfacial layer has recently attracted more and more attention due to its much higher Li^+ conductivity (~10^{-3} S cm^{-1} at room temperature) than LiF[19] and thermodynamic stability against Li metal[20] as well as negligible partial electronic conductivity.[21] Goodenough and co-workers have shown that introducing a thin Li_3N layer on the surface of a garnet electrolyte can minimize overpotential and enable durable Li plating/stripping.[19] However, Li_3N suffers from poor chemical/environmental stability owing to its sensitivity with ambient moisture and reactivity with commonly used aprotic polar solvents (e.g., NMP).[22] In addition, the electrochemical stability of Li_3N is poor, as it tends to decompose at voltages higher than 0.44 V vs. Li/Li^+.[23] Therefore, new strategies to build chemically, electrochemically, mechanically, and environmentally stable interlayers are desired.[24,25] Melamine (denoted as MA), widely known for its ultrahigh nitrogen content, can be used as a N source after high-temperature treatment to enhance the activity of N species and electron conductivity. Consequently, MA is deliberately chosen for building an electrode interface that may provide an N-rich layer and offer high Li^+ conductivity.

In this study, we report in situ construction of an ultra-robust and lithiophilic Li-enriched Li-N interlayer on Ge anodes via a facile and scalable wet-chemical reaction between melamine and Li^+. Such a uniform Li-enriched interlayer effectively protects the Ge anode against electrolyte solvent, and forms a thin SEI. In addition, Li-enriched structure can be considered as an affluent Li^+ reservoir to promote efficient Li^+ conduction. Moreover, thanks to the

improved wettability of the Li-N interlayer, the migration and diffusion kinetics of Li^+ can be further improved. Hence, the introduction of such Li-N interlayer with good Li^+ conductivity, thinner characteristics, and flexibility significantly enhanced the stability of the Ge anode during prolonged cycling.

Structure design and characterization of Li-enriched Li-N interlayer. The construction of a Li-enriched Li-N interlayer on Ge anodes was shown in Scheme 1. Firstly, MA was homogeneously coated on the surface of Ge by immersing bare Ge into an MA solution. Then, MA molecules self-assembled on the surface of Ge due to a strong interaction between Ge and MA via the formation of strong Ge-N bond and denoted as MA@Ge. Secondly, the Li-enriched Li-N interlayer was formed in situ during discharge/charge via the reaction of Li^+ with the -NH_2 of MA. Note that the potential is a critical factor to trigger such a reaction as the direct immersion of MA@Ge with Li-containing electrolytes did not form any Li-N bonds (Figure S1). The resultant Li-enriched Li-N interlayer can therefore serve as a versatile protective nanoshield to promote the battery performance of Ge anodes. Compared to the powder X-ray diffraction (PXRD) pattern of standard MA, there are no obvious peaks of crystalline MA in the MA@Ge, indicating that the MA layer is very thin or exists in an amorphous phase (Figure S2a, b). In addition, both bare Ge and MA@Ge have a hierarchical micro/nanostructure (Figure S2c-f), including micrometer-sized particles (10-20 μm) which composed of nanometer-sized particles. Transmission electron microscopy (TEM) characterization further shows that the MA@Ge has a core shell-like nanostructure (Figure 1a and Figure S3), with each core having an amorphous MA shell about 5 nm thick (Figure 1b). A typical high-resolution TEM (HRTEM) image shows that the d-spacing is measured to be 0.340 nm (Figure S3c), which matches well with the d-spacing of the Ge (111) plane. X-ray photoelectron spectroscopy (XPS) result in Figure 1c shows the coexistence of the peaks of -NH_2 and pyridinic N (from MA, see Figure S1a). Moreover, the deconvolution area of -NH_2 has an obvious decrease in MA@Ge compared to pure MA, and Ge-N can be obviously observed, demonstrating that Ge is able to interact with

MA. The strong interaction between Ge and MA was further evidenced by density functional theory (DFT) calculations. As shown in Figure 1d, MA can easily absorb on the surface of Ge (111) with a high binding energy of -1.22 eV, triggering the self-assembly and homogeneous coating of MA molecules on the surface of Ge.

Electrochemical characterization. The advantages of the Li-enriched Li-N interlayer were verified by electrochemical tests within 0.01-2 V. The MA@Ge electrode demonstrates a better rate performance compared with bare Ge (Figure 2a-c). The corresponding average discharge capacities of MA@Ge (1325, 1307, 1251, 1187, 1060 mAh g^{-1}) at various current densities are all much higher than those of bare Ge (1272, 1102, 990, 781, and 689 mAh g^{-1}). In addition, a relatively flat voltage plateau in the Galvanostatic discharge-charge (GDC) curves is well maintained even at 2 A g^{-1} (Figure 2b). Figure 2d-f shows the cycling performances and GDC curves of the MA@Ge and bare Ge electrodes at 500 mA g^{-1}. After 300 cycles of discharge/charge, the reversible capacity of the MA@Ge electrode is 1176 mAh g^{-1}, in contrast to just 65 mAh g^{-1} for Ge without MA coating. The corresponding areal capacities of the MA@Ge and bare Ge electrodes are displayed in Figure S4a. The MA@Ge electrode exhibits 1.05 mAh cm^{-2} after 300 cycles at 0.5 mA cm^{-2}, which is much higher than the bare Ge counterpart. Simultaneously, the improvement of rate performance in areal capacities is also observed in the case of the MA@Ge electrode in comparison with the bare Ge counterpart (Figure S4b).

When the current density was increased to 1 A g^{-1}, the reversible capacity of the MA@Ge electrode is 1024 mAh g^{-1} after 300 cycles (Figures S5a), accounting for 80% capacity retention. Similarly, the reversible capacity is 921.1 mAh g^{-1} after 200 cycles at 2 A g^{-1} (Figures S5b), corresponding to a capacity retention of 78%. In contrast, the capacity retentions are only 2% at 1 A g^{-1} and 3% at 2 A g^{-1} for the bare Ge electrodes, respectively. In comparison, this result rivalled most of Ge-based anodes with or without surface coating (Table S1).[14,24,29-31,35,36]

Strikingly, our preliminary data (Figures S6 and S7) shows that the strategy of constructing an Li-N interlayer is also appropriate for Si anode.

The Electrochemical impedance spectroscopy (EIS) characterization showed that the interfacial charge transfer resistance of MA@Ge is significantly reduced compared to bare Ge (Figure S8 and Table S2). Cyclic voltammetry (CV) characterization has further confirmed the fast Li^+ diffusion coefficient and more efficient Li^+ conduction of MA@Ge electrode over bare Ge electrode (Figure S9).

Structure characterization during discharge/charge. Figure 3a shows the *In situ* PXRD of the MA@Ge electrode during discharge-charge processes. The peaks without color unchanged are belonging to Be window and the home-made in situ cell. The peak with color change reflects a clear phase transition, which is different from most cathode materials that undergo less obvious phase transition during charge-discharge.[26,27] A broad peak emerged at 20.0-25.0°, which corresponds to lithiation to 0.35 V vs. Li/Li^+, and suggest the formation of amorphous Li_xGe phases. To get a clear signal, the mass of active materials is as high as ~ 5.0 mg cm^{-2}, leading to still observed Ge peaks at the end of lithiation, but the intensity is obviously decreased. During charge, the broad peak disappeared due to the delithiation of Li_xGe to Ge. When charged to 2.0 V in the 2nd charge, several new peaks (17.5°, 20.6°, 25.6°, 26.1°, etc.) belonging to crystalline LiMA compounds emerged, which is consistent with the previously reported Li-MA complex.[28]

Figure 3b shows normalized Ge K-edge X-ray near-edge spectroscopy (XANES) spectra for the bare Ge and MA@Ge at OCV, discharge to 0.2 and 0.02 V, and charge to 0.15 and 2.0 V during the 1st cycle. The peak position of the MA@Ge at OCV is consistent with that of bare Ge (Figure S10a), which indicates that the as-prepared MA@Ge comprises the metallic phase of Ge. The peak intensity of the white line (~11.12 keV) is proportional to the concentration of the unoccupied 4p orbital of Ge.[29,30] As the lithiation reaction occurs, it can be observed that the white line of Ge shifted to lower energy during the discharge process, which became broader,

due to the formation of amorphous Li−Ge phase. Therefore, it can lead to an electron-shielding effect on the Ge, which benefits to lower the shift of the first-derivative peak to lower the energy exciting the Ge electrons from 1s to 4p. As shown in Figure 3b, with the discharge reaction occurring from 0.2 V to 0.01 V, the intensity of the white line decreases and the Ge K-edge shifts to a lower energy, due to the reduction of Ge during discharge. Reversibly, when charging back to 2 V, all the peaks and edges return to the original status. These results clearly indicate that the lithiation/delithiation is highly reversible during the first cycle (see detail in Figure S10b).

As further shown in Figure 3c and Figure S11a, a characteristic peak at ~2.1 Å corresponding to metallic Ge-Ge bonds can be observed in the Ge K-edge extended X-ray fine structure (EXAFS) spectra of pristine MA@Ge. With the deepening of discharge depth, especially in full the discharge stage (discharge to 0.02 V), the signal of the 1st, 2nd, and 3rd Ge-Ge shells decrease, and even disappear, illustrating that Ge-Ge metallic-bond cleavage is occurring. During the delithiation process, the 1st Ge-Ge coordination sphere intensity cannot be fully recovers, and the higher-order shells completely disappeared (see Figure S11b), indicating the amorphization of Ge after delithiation.[31] This result is consistent with the in situ PXRD and XANES results, which can be confirmed by the TEM image of Figure 3d after cycling for 9 cycles. It is well known that utilization of amorphous materials can accommodate the stress at the phase boundaries, resulting in homogeneous volume variation and prolonged cycle life.[32-34] Figure 3d also clearly shows that the in situ constructed Li-N interlayer is well maintained without breaking or thickening after cycling, confirming its high mechanical integrity.

The mechanism of Li^+ conduction in the in situ formed Li-enriched Li-N interlayer.

Figures 4a-f display the deconvolution of the N 1s XPS spectra of the MA@Ge electrode at different discharge/charge states. With the occurrence of lithiation/delithiation reactions, Li-N

product becomes more and more dominant in the interface and the signal of -NH_2 gradually weakens, indicating that -NH_2 of MA is substituted by Li^+ to form Li-N. The results illustrate that the Li-N bond is formed in situ during the cycling and subsequent cycles (Figure S12). Specifically, we employed isolated Li atoms as reference states to probe the interaction between Li^+ and MA (see details in Figure S13), which confirmed the preferable coordination between Li^+ and -NH_2.

We further synthesized a LiMA compound by a chemical reaction between MA and LiOH (see detail in Figure S14). The N 1s XPS peak in the as-prepared Li-N compound is in good accordance with the above XPS results derived from MA@Ge in Figures 4a-f. This result verifies that the MA is indeed converted to a Li-enriched Li-N interlayer during discharge/charge. The result also indicates the possibility of constructing a Li-N nanoshield via chemical reactions on the surface of electrode materials. Compared to Li_3N, the Li-enriched Li-N interlayer has a high chemical stability and electrochemical window (Figures S15 and S16), implying that LiMA may be more suitable for interface engineering than Li_3N.

The in situ SEM was employed to track the morphological of a single MA@Ge particle during discharge/charge processes.[35, 36] Figures 5a and Figure S17 illustrate the morphology of a MA@Ge particle under low current (150 pA) at the first cycle. After the full lithiation, the volume expands to 294%, significantly lower than the bare Ge particle expansion in our previous result (360%).[14] Accompanied by the extraction of Li atoms during charge, the volume contracts to 141% at the end of first charge. Moreover, we carried out in situ SEM measurements at the 3rd cycle (Figure S17a) and the 9th cycle (Figure S17b) and calculated their volume change., which are about 147% (3rd cycle) and 152% (9th cycle), respectively. Thus, the Li-enriched Li-N interlayer could significantly mitigate the volume changes of Ge during repeated lithiation/delithiation. In addition, the particle size evolution at different discharge/charge stages in two directions were analyzed (Figure S17c), which demonstrates that the size changes in the two directions are almost kept same speed, indicating that the

lithiation/delithiation of Li^+ in the particles are synchronous in all directions.[37,38]

The MA layer can hinder a direct plating of lithium on the tips of Ge to avoid the dendrite growth.[39] The electrolyte wettability of the MA coating layer was measured to explore the interfacial lithiophilic properties. The contact angle between the MA@Ge substrate and electrolyte decreased to 17.89°, which was much smaller than that of bare Ge (41.27°), indicating that the wettability of the MA@Ge substrate with electrolyte is significantly enhanced (Figures 5b). The wettability of the electrolyte can affect the uptake amount of electrolyte and thus the distribution of Li^+ flux on the whole anode surface during the cycling process.[40] Such a good electrolyte wettability from the MA layer can remarkably improve the diffusion of Li^+ across the interface, which can thus build an ultra-lithiophilic interface on Ge electrode. Furthermore, the as-synthesized Li-N interlayer via chemical reaction also showed a small contact angle of 15.81°, further demonstrating our concept.

Characterization of interface. We further utilized Online Electrochemical Mass Spectrum (OEMS) measurement to check the possible gaseous byproducts, formed by the redox reaction of electrolyte solvent in the first discharge process.[41] Figures 5c-d and S18 display the gas product of CO_2 and CO, which m/z values are 44 and 28, respectively, of the MA@Ge and bare Ge electrodes .[42] It is worth noting that the signal of m/z equal to 28 is not from N_2 (Figure S19). The intensity of CO from MA@Ge electrode is significantly lower than that of the bare Ge electrode, confirming that the decomposing of solvent molecules in the MA@Ge is significantly suppressed. As shown in Table S3, the intensity and area of these peaks assigned to bare Ge are much higher than those of MA@Ge. OEMS results indicate that a much thinner SEI can be formed on the MA@Ge electrode, which favors transport of Li^+. This is evidenced by the XPS results, in which the Ge 2p spectrum demonstrates Li-Ge signal for the MA@Ge electrode (Figure 20a), while no Ge signal for the pure Ge electrode can be observed due to the formation of a thick SEI (Figure 20b). Furthermore, the C 1s spectrum of RO-CO_2Li and C-O-C are formed by the decomposing of electrolyte solvents (Figure S21).

The intensities of RO-CO_2Li and C-O-C peaks in the MA@Ge are much lower than that of the bare Ge electrode according to the reference peak of 284.8 eV.

In summary, we performed a novel and facile interface engineering approach for Ge anodes by in situ construction of an ultra-robust and lithiophilic Li-enriched Li-N nanoshield. The Li-N nanoshield-modified Ge electrode exhibits good cycle stability and an improved rate capability thanks to the introduction of the Li-N nanoshield, which: 1) effectively suppresses the volume changes during cycling, as evidenced by in situ SEM experiment; 2) significantly prevents the attack of the electrolyte solvents, as evidenced by XPS and OEMS results, and forms a thinner and robust SEI; and 3) remarkably facilitates interfacial Li^+ transport kinetics thanks to its high Li^+ conductivity and Li-enriched reservoir. Our methodology provides a new concept and direction to designing rechargeable batteries with high performance.

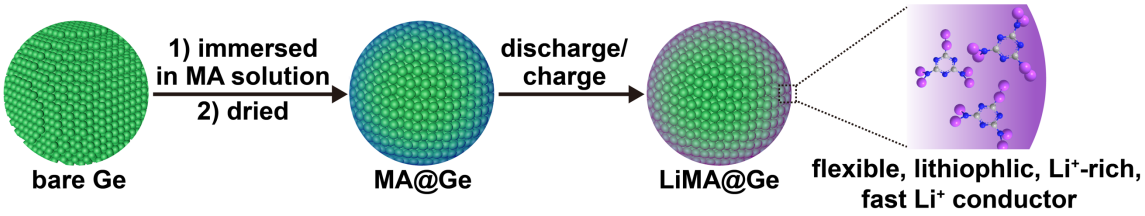

Scheme 1. Illustration of the synthesis of MA@Ge and the transformation of the Li-ion conduction layer. Blue, green, gray, and purple represent N, Ge, C, and Li, respectively.

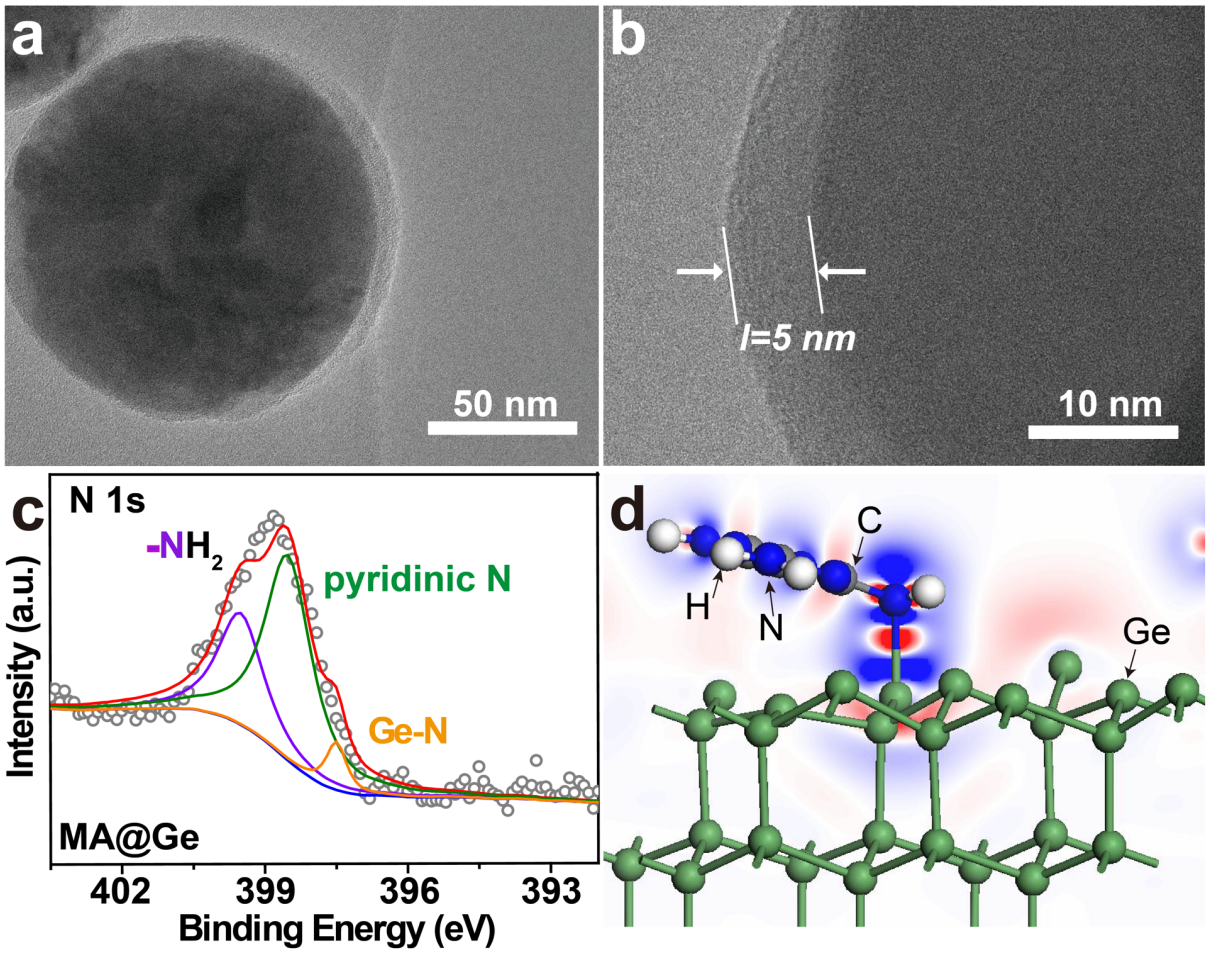

Figure 1. Fabrication and characterization of MA@Ge. (a, b) TEM and (c) N 1s XPS spectra of the MA@Ge. (d) The binding energy between MA and the Ge (111) surface by using DFT calculations.

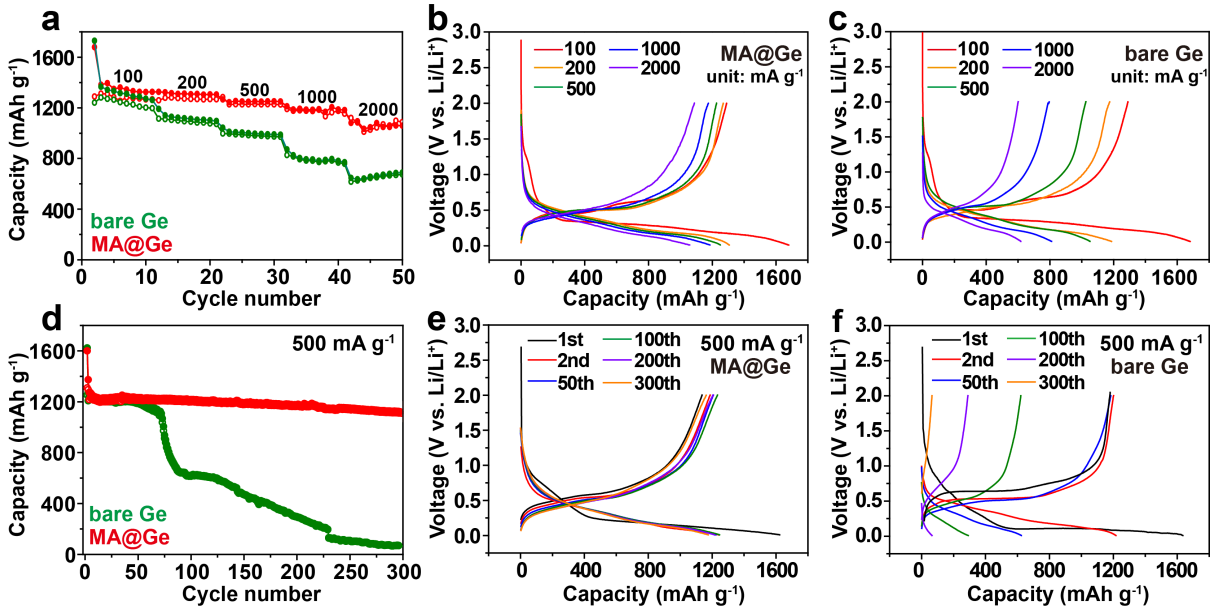

Figure 2. Electrochemical performances of MA@Ge and bare Ge electrodes. (a) Rate performances and (b, c) GDC curves of bare Ge and MA@Ge at different current densities, (d) Cycling performances and (e, f) GDC curves at a current density of 500 mA g^{-1}.

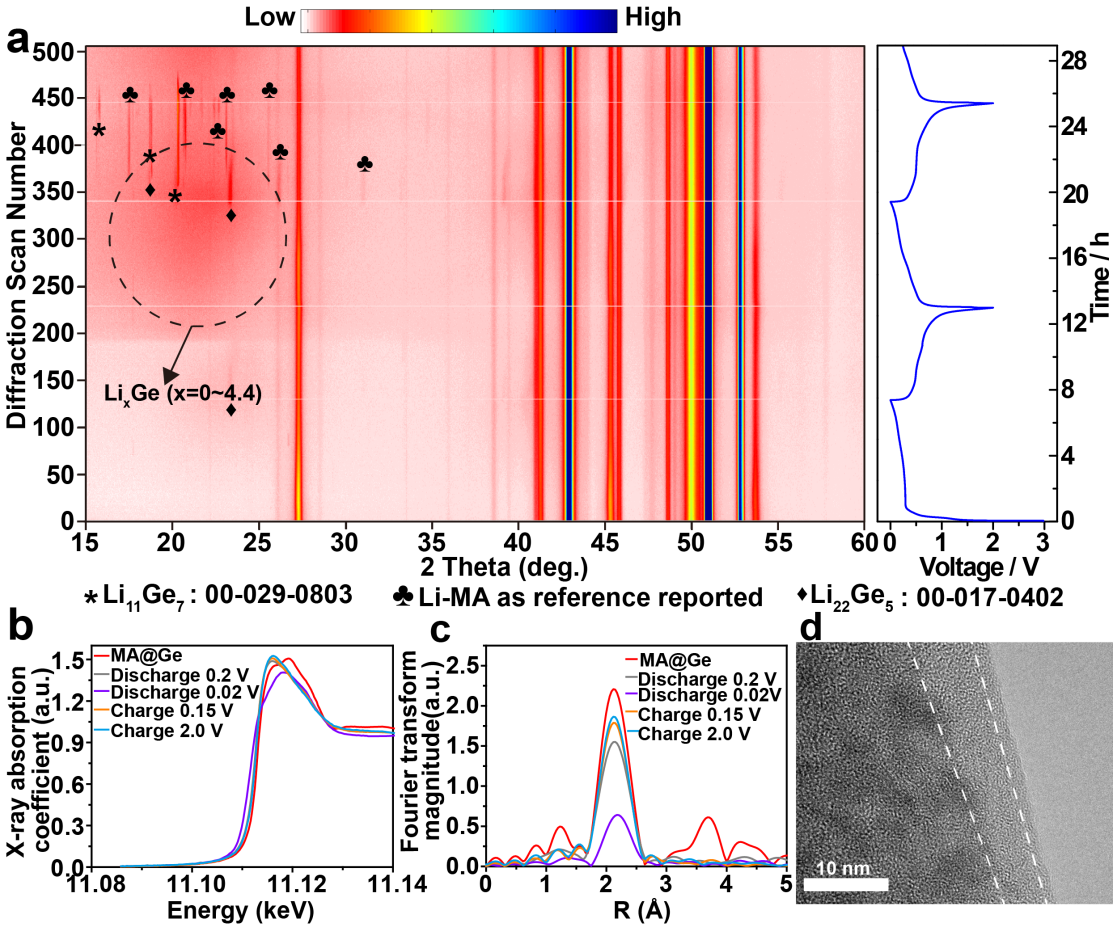

Figure 3. (a) The in situ PXRD patterns of the MA@Ge electrode and the corresponding lithiation/delithiation curves of the initial two cycles at 300 mA g^{-1}. (b) Normalized Ge K-edge XANES and (c) Fourier transform (FT) magnitudes of the Ge K-edge k3-weighted EXAFS spectra for the MA@Ge electrode at OCV, discharge to 0.2 V, 0.02 V, and charge to 0.15 V and 2.0 V for MA@Ge; (d) TEM images of MA@Ge after 9th cycle.

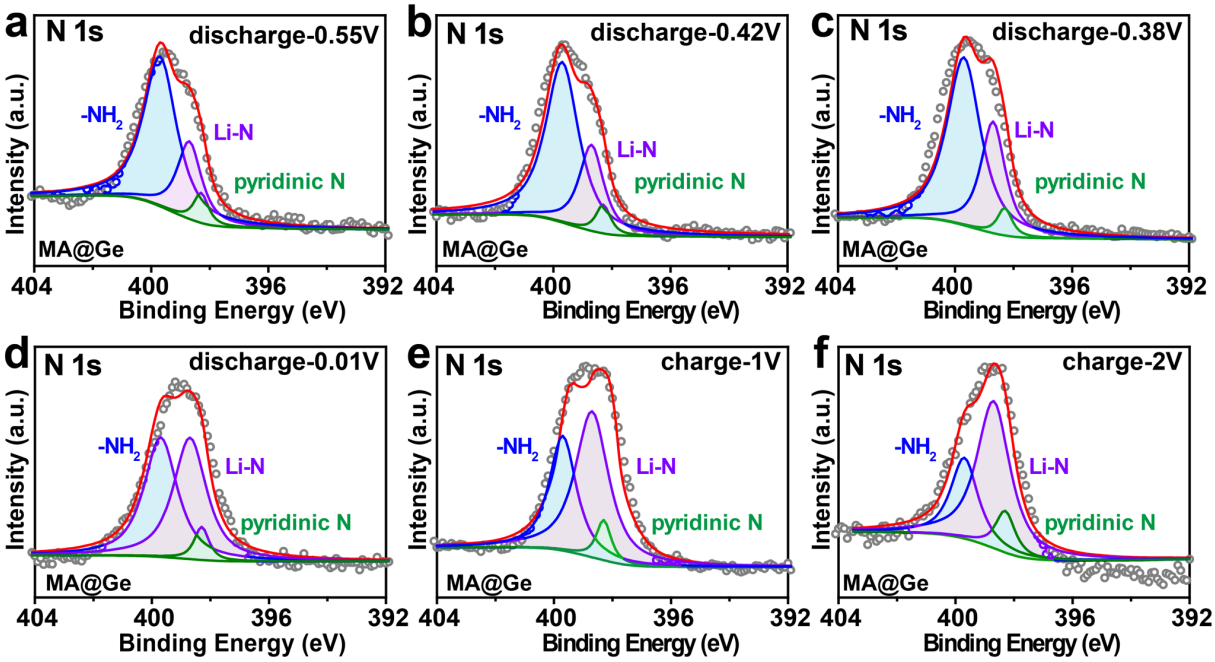

Figure 4. XPS analysis of N 1s at different discharge stages: (a) 0.55 V, (b) 0.42 V, (c) 0.38 V and (d) 0.01 V for MA@Ge electrodes. N 1s at different charge stages (e) 1.0 V and (f) 2.0 V for MA@Ge electrodes.

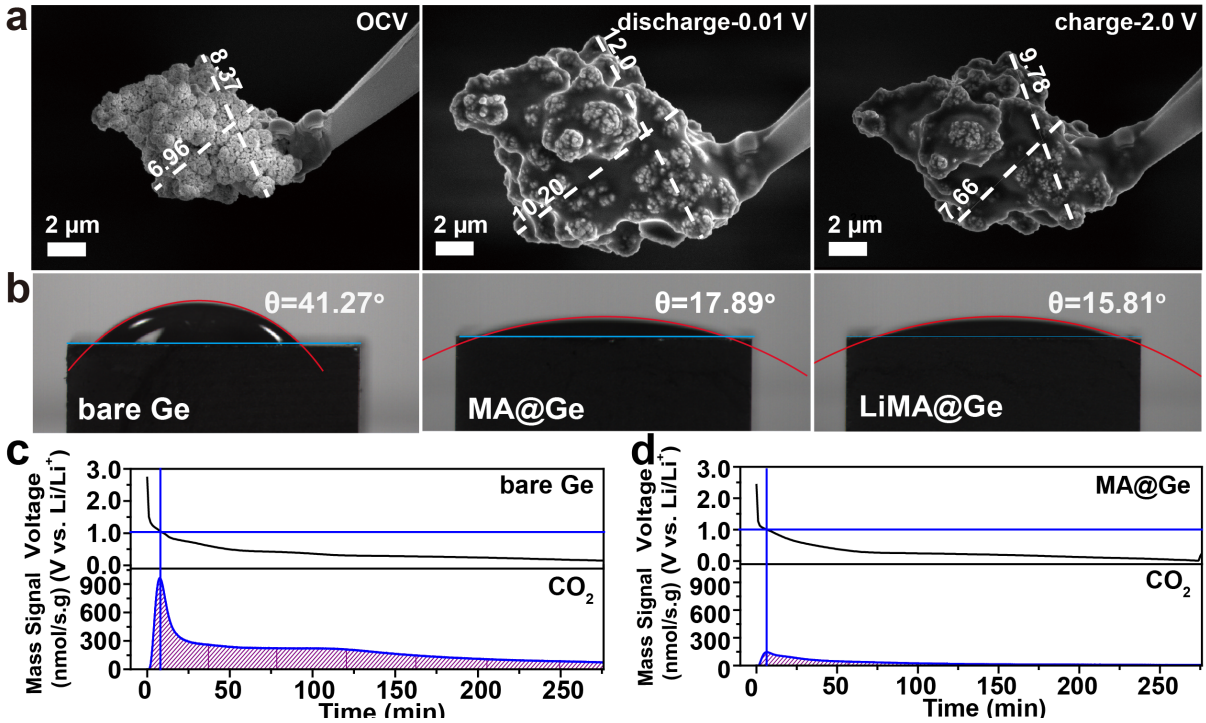

Figure 5. (a) The morphologies of a MA@Ge particle at OCV, discharge to 0.01 V, charge to 2.0 V state. (b) Contact angles of the electrolyte and the bulk Ge, MA@Ge, and LiMA@Ge. Plots of CO_2 (m/z = 44) evolution of (c) bare Ge and (d) MA@Ge electrodes for the initial 275 min during the 1st lithiation process.

ASSOCIATED CONTENT

Supporting Information: Experimental Methods, Structural and composition characterizations of the MA@Ge composite, electrochemical measurements of the MA@Ge composite, in situ XRD and OEMS measurements and Computational details of MA@Ge composite electrodes.

AUTHOR CONTRIBUTIONS

†B.-Q. X and X. Z. contributed equally to this work.

AUTHOR INFORMATION

Corresponding Authors

*E-mail: xug@anl.gov

*E-mail: amine@anl.gov

*E-mail: kefs@whu.edu.cn

Notes

The authors declare no competing financial interest.

ACKNOWLEDGMENT

We thank Prof. Hexiang Deng and Dr. Hengjiang Cong from Wuhan University for their invaluable help. This work was sponsored by National Nature Science Foundation of China (21773176, 21403157) and the Fundamental Research Funds for the Central Universities (2042019kf0200). F.S.K. acknowledges the Large-scale Instrument and Equipment Sharing Foundation of Wuhan University. DFT calculations in this paper were done on the supercomputing system in the Supercomputing Center of Wuhan University. This work was also partially supported by the National Science Foundation under Grant Number CBET1408751. Research at Argonne National Laboratory was funded by the U.S. Department

of Energy (DOE), Vehicle Technologies Office. Use of the Advanced Photon Source and the Center for Nanoscale Materials, both Office of Science user facilities, was supported by the DOE, Office of Science and Office of Basic Energy Sciences, under contract no. DE-AC02-06CH11357. K.A. and G.L.X. are also thankful for the support from Clean Vehicles, US-China Clean Energy Research Centre (CERC-CVC2).

REFERENCES

(1) Song, K.; Liu, C.; Mi, L.; Chou, S.; Chen, W.; Shen, C. Recent Progress on the Alloy-Based Anode for Sodium-Ion Batteries and Potassium-Ion Batteries. *Small* **2019**, *15*, 1903194.

(2) An, W. L.; Gao, B. A.; Mei, S. X; Xiang, B.; Fu, J. J.; Wang, L.; Zhang, Q. B.; Chu, P. K.; Huo, K. F. Scalable Synthesis of Ant-Nest-Like Bulk Porous Silicon for High-Performance Lithium-Ion Battery Anodes. *Nat. Commun.* **2019**, *10*, 1447.

(3) Zhang, Z. L.; Wang, Y. H.; Ren, W. F.; Tan, Q. Q.; Chen, Y. F.; Li, H.; Zhong, Z. Y.; Su, F. B. Scalable Synthesis of Interconnected Porous Silicon/Carbon Composites by the Rochow Reaction as High-Performance Anodes of Lithium Ion Batteries. *Angew. Chem. Int. Ed.* **2014**, *53*, 5165-5169.

(4) Liang, J.; Li, X.; Hou, Z.; Zhang, W.; Zhu, Y.; Qian, Y. A Deep Reduction and Partial Oxidation Strategy for Fabrication of Mesoporous Si Anode for Lithium Ion Batteries. *ACS Nano* **2016**, *10*, 2295-2304.

(5) Szczech, J. R.; Jin, S. Nanostructured Silicon for High Capacity Lithium Battery Anodes. *Energy Environ. Sci.* **2011**, *4*, 56-72.

(6) Ji, L. W.; Lin, Z.; Alcoutlabi, M.; Zhang, X. W. Recent Developments in Nanostructured Anode Materials for Rechargeable Lithium-Ion Batteries. *Energy Environ. Sci.* **2011**, *4*, 2682-2699.

(7) Ko, J.; Yoon, Y. S. Recent Progress in LiF Materials for Safe Lithium Metal Anode of Rechargeable Batteries: Is LiF the Key to Commercializing Li Metal Batteries? *Ceram. Int.* **2019**, *45*, 30-49.

(8) Li, F.S.; Wu, Y. S.; Chou, J.; Winter, M.; Wu, N. L. A Mechanically Robust and Highly Ion-Conductive Polymer-Blend Coating for High-Power and Long-Life Lithium-Ion Battery Anodes. *Adv. Mater.* **2014**, *27*, 130-137.

(9) Schroder, K.; Alvarado, J.; Yersak, T. A.; Li, J.; Dudney, N.; Webb, L. J.; Meng, Y. S.; Stevenson, K. J. The Effect of Fluoroethylene Carbonate as an Additive on the Solid Electrolyte Interphase on Silicon Lithium-Ion Electrodes. *Chem. Mater.* **2015**, *27*, 5531-5542.

(10) Yamada, Y.; Wang, J. H.; Ko, S.; Watanabe, E.; Yamada, A. Advances and Issues in Developing Salt-Concentrated Battery Electrolytes. *Nat. Energy* **2019**, *4*, 269-280.

(11) Fan, X.; Chen, L.; Ji, X.; Deng, T.; Hou, S.; Chen, J.; Zheng, J.; Wang, F.; Jiang, J.; Xu, K.; Wang, C. Highly Fluorinated Interphases Enable High-Voltage Li-Metal Batteries. *Chem* **2018**, *4*, 174-185.

(12) Yang, G.; Li, Y.; Liu, S.; Zhang, S.; Wang, Z.; Chen, L. LiFSI to Improve Lithium Deposition in Carbonate Electrolyte. *Energy Storage Mater.* **2019**, *23*, 350-357.

(13) Suo, L.; Xue, W.; Gobet, M.; Greenbaum, S. G.; Wang, C.; Chen, Y.; Yang, W.; Li, Y.; Li, J. Fluorine-Donating Electrolytes Enable Highly Reversible 5-V-Class Li Metal Batteries. *Proc. Natl. Acad. Sci.* **2018**, *115*, 1156-1161.

(14) Xiong, B.-Q.; Zhou, X.; Xu, G.-L.; Liu, Y.; Zhu, L.; Hu, Y.; Shen, S.-Y.; Hong, Y.-H.; Wan, S.-C.; Liu, X.-C.; Liu, X.; Chen, S.; Huang, L.; Sun, S.-G.; Amine, K.; Ke, F.-S. Boosting Superior Lithium Storage Performance of Alloy-Based Anode Materials via Ultraconformal Sb Coating-Derived Favorable Solid-Electrolyte Interphase. *Adv. Energy Mater.* **2020**, *10*, 1903186.

(15) Pan, J.; Cheng, Y.-T.; Qi, Y. General Method to Predict Voltage-Dependent Ionic Conduction in a Solid Electrolyte Coating on Electrodes. *Phys. Rev. B* **2015**, *91*, 134116.

(16) Huang, W.; Wang, H.; Boyle, D. T.; Li, Y.; Cui, Y. Resolving Nanoscopic and Mesoscopic Heterogeneity of Fluorinated Species in Battery Solid-Electrolyte Interphases by Cryogenic Electron Microscopy. *ACS Energy Lett*. **2020**, *5*, 1128-1135.

(17) Yildirim, H.; Kinaci, A.; Chan, M. K. Y.; Greeley, J. P. First-Principles Analysis of Defect Thermodynamics and Ion Transport in Inorganic SEI Compounds: LiF and NaF. *ACS Appl. Mater. Interfaces* **2015**, *7*, 18985-18996.

(18) He, M. F.; Guo, R.; Hobold, G. M.; Gao, H. N.; Gallant, B. M. The Intrinsic Behavior of Lithium Fluoride in Solid Electrolyte Interphases on Lithium. *Proc. Natl. Acad. Sci.* **2020**, *117*, 73-79.

(19) Xu, H.; Li, Y.; Zhou, A.; Wu, N.; Xin, S.; Li, Z.; Goodenough, J. B. Li_3N-Modified Garnet Electrolyte for All-Solid-State Lithium Metal Batteries Operated at 40 °C. *Nano Lett.* **2018**, *18*, 7414-7418.

(20) Fan, X.; Ji, X.; Han, F.; Yue, J.; Chen, J.; Chen, L.; Deng, T.; Jiang, J.; Wang, C. Fluorinated Solid Electrolyte Interphase Enables Highly Reversible Solid-State Li Metal Battery. *Sci. Adv.* **2018**, *4*, eaau9245.

(21) Alpen, U. v. Li_3N: A Promising Li Ionic Conductor. *J. Solid State Chem.* **1979**, *29*, 379-392.

(22) Sun, Y.; Li, Y.; Sun, J.; Li, Y.; Pei, A.; Cui, Y. Stabilized Li_3N for Efficient Battery Cathode Prelithiation. *Energy Storage Mater.* **2017**, *6*, 119-124.

(23) Park, K. Yu, B.-C. Goodenough, J. B. Li_3N as a Cathode Additive for High-Energy-Density Lithium-Ion Batteries. *Adv. Energy Mater.* **2016**, *6*, 1502534.

(24) Gao, X.; Luo, W.; Zhong, C.; Wexler, D.; Chou, S.-L.; Liu, H.-K.; Shi, Z.; Chen, G.; Ozawa, K.; Wang, J.-Z. Novel Germanium/Polypyrrole Composite for High Power Lithium-Ion Batteries. *Sci. Rep.* **2014**, *4*, 6095.

(25) Li, F. S.; Wu, Y. S.; Chou, J.; Winter, M.; Wu, N. L. A Mechanically Robust and Highly Ion-Conductive Polymer-Blend Coating for High-Power and Long-Life Lithium-Ion Battery Anodes. *Adv. Mater.* **2015**, *27*, 130-137.

(26) Li, J.; Shunmugasundaram, R.; Doig, R.; Dahn, J. R. In Situ X-ray Diffraction Study of Layered Li–Ni–Mn–Co Oxides: Effect of Particle Size and Structural Stability of Core–Shell Materials. *Chem. Mater.* **2016**, *28*, 162-171.

(27) Li, W.; Asl, H. Y.; Xie, Q.;Mathiram, A. Collapse of $LiNi_{1-x-y}Co_xMn_yO_2$ Lattice at Deep Charge Irrespective of Nickel Content in Lithium-Ion Batteries. *J. Am. Chem. Soc.* **2019**, *141*, 5097-5101.

(28) Shetty V. R.; Suresh, G. S.; Mahadevan, K. M. Electrochemical Activities of Melamine and Its Applications in Aqueous Rechargeable Lithium Ion Batteries. *Indian J. Adv. Chem. Sci.* **2016**, *S1*, 263-266.

(29) Lee, H.; Kim, M. G.; Choi, C. H.; Sun, Y. K.; Yoon, C. S.; Cho, J. Surface-Stabilized Amorphous Germanium Nanoparticles for Lithium-Storage Material. *J. Phys. Chem. B* **2005**, *109*, 20719-20723.

(30) Lim, L. Y.; Liu, N.; Cui, Y.; Toney, M. F. Understanding Phase Transformation in Crystalline Ge Anodes for Li-Ion Batteries. *Chem. Mater.* **2014**, *26*, 3739-3746.

(31) Silberstein, K. E.; Lowe, M. A.; Richards, B.; Gao, J.; Hanrath, T.; Abruna, H. D. Operando X-ray Scattering and Spectroscopic Analysis of Germanium Nanowire Anodes in Lithium Ion Batteries. *Langmuir* **2015**, *31*, 2028-2035.

(32) Han, J. H.; Hirata, A.; Du, J.; Ito, Y.; Fujita, T.; Kohara, S.; Ina, T.; Chen, M. W. Intercalation Pseudocapacitance of Amorphous Titanium Dioxide@Nanoporous Graphene for High-Rate and Large-Capacity Energy Storage. *Nano Energy*, **2018**, *49*, 354-362.

(33) Feng, J.; Wang, H.; Hu, Z.; Zhang, M.; Yang, X.; Yuan, R.; Chai, Y. Hollow Co_2SiO_4 Microcube with Amorphous Structure as Anode Material for Construction of High Performance Lithium Ion Battery. *Ceram. Int.* **2019**, *45*, 13369-13375.

(34) Wu, H. Y.; Qin, M. L.; Wang, W.; Cao, Z. Q.; Liu, Z. W.; Yu, Q. Y.; Lao, C. Y.; Zhang, D. Y.; Jia, B. R.; He, D. L.; Liu, T. T.; Volinsky, A. A.; Cao, P.; Qu, X. H. Ultrafast Synthesis of Amorphous VO_x Embedded into 3D Strutted Amorphous Carbon Frameworks-Short-Range Order in Dual-Amorphous Composites Boosts Lithium Storage. *J. Mater. Chem. A* **2018**, *6*, 7053-7061.

(35) Zhou, X.; Li, T.; Cui, Y.; Meyerson, M. L.; Mullins, C. B.; Liu, Y.; Zhu, L. In Situ Focused Ion Beam-Scanning Electron Microscope Study of Crack and Nanopore Formation in Germanium Particle During (De)Lithiation. *ACS Appl. Energy Mater.* **2019**, *2*, 2441-2446.

(36) Liang, W.; Yang, H.; Fan, F.; Liu, Y.; Liu, X. H.; Huang, J. Y.; Zhu, T.; Zhang, S. Tough Germanium Nanoparticles under Electrochemical Cycling. *ACS Nano* **2013**, *7*, 3427-3433.

(37) Luo, L.; Yang, H.; Yan, P.; Travis, J. J.; Lee, Y.; Liu, N.; Molina Piper, D.; Lee, S.-H.; Zhao, P.; George, S. M.; Zhang, J.-G.; Cui, Y.; Zhang, S.; Ban, C.; Wang, C.-M. Surface-Coating Regulated Lithiation Kinetics and Degradation in Silicon Nanowires for Lithium Ion Battery. *ACS Nano* **2015**, *9*, 5559-5566.

(38) Sandu, G.; Brassart, L.; Gohy, J.-F.; Pardoen, T.; Melinte, S.; Vlad, A. Surface Coating Mediated Swelling and Fracture of Silicon Nanowires during Lithiation. *ACS Nano* **2014**, *8*, 9427-9436.

(39) Ding, F.; Xu, W.; Graff, G. L.; Zhang, J.; Sushko, M. L.; Chen, X.; Shao, Y.; Engelhard, M. H.; Nie, Z.; Xiao, J.; Liu, X.; Sushko, P. V.; Liu, J.; Zhang, J. G., Dendrite-Free Lithium Deposition via Self-Healing Electrostatic Shield Mechanism. *J. Am. Chem. Soc.* **2013**, *135*, 4450-4456.

(40) Tan, S. J.; Yue, J.; Hu, X. C.; Shen, Z. Z.; Wang, W. P.; Li, J. Y.; Zuo, T. T.; Duan, H.; Xiao, Y.; Yin,Y. X.; Wen, R.; Guo, Y. G. Nitriding-Interface-Regulated Lithium Plating Enables Flame-Retardant Electrolytes for High-Voltage Lithium Metal Batteries. *Angew. Chem. Int. Ed.* **2019**, *58*, 7802-7807.

(41) Shen, S.; Hong, Y.; Zhu, F.; Cao, Z.; Li, Y.; Ke, F.; Fan, J.; Zhou, L.; Wu, L.; Dai, P.; Cai, M.; Huang, L.; Zhou, Z.; Li, J.; Wu, Q.; Sun, S. Tuning Electrochemical Properties of Li-Rich Layered Oxide Cathodes by Adjusting Co/Ni Ratios and Mechanism Investigation Using *In Situ* X-ray Diffraction and Online Continuous Flow Differential Electrochemical Mass Spectrometry. *ACS Appl. Mater. Interfaces* **2018**, *10*, 12666-12677.

(42) Xu, W.; Wang, J.; Ding, F.; Chen, X.; Nasybulin, E.; Zhang, Y.; Zhang, J.-G. Lithium Metal Anodes for Rechargeable Batteries. *Energy Environ. Sci.* **2014**, *7*, 513-537.